EUROPEAN ORGANIZATION FOR NUCLEAR RESEARCH

CERN/EP 87-118
3 July 1987

AN IMPACT PARAMETER ANALYSIS OF PROTON-PROTON ELASTIC AND INELASTIC INTERACTIONS AT 360 GeV/c

EHS-RCBC Collaboration

J.L. Bailly[9], S. Banerjee[1], F. Bruyant[3], B. Buschbeck[12], C. Caso[5], H. Dibon[12], F.J. Diez-Hedo[8], A. Ferrando[8], F. Fontanelli[5], Yu.A. Golubkov[10], R. Hamatsu[7a], P. Herquet[9], J. Hrubec[12], Y. Iga[7a], Yu. Ivanyushenkov[11], N.S. Khalatyan[11], E.P. Kistenev[11], S. Kitamura[7a], J.M. Kohli[4], V.M. Kubik[11], D. Kuhn[6], B.B. Levchenko[10], J. MacNaughton[12], L. Montanet[3], G. Neuhofer[3], A. Ohta[7a], G. Pinter[2], P. Porth[12], R. Raghavan[1], K. Rasner[6], T. Rodrigo[8], J.M. Salicio[8], J.B. Singh[4], S. Squarcia[5], K. Takahashi[7b], L.A. Tikhonova[10], U. Trevisan[5], T. Tsurugai[7a] and G.V. Zholobov[11]

1 Tata Institute of Fundamental Research, Bombay, India
2 Central Research Institute for physics, Budapest, Hungary
3 CERN, European Organization for Nuclear Research, Geneva, Switzerland
4 Panjab University, Chandigarn, India
5 Istituto di Fisica, Università di Genova and INFN, Genova, Italy
6 Institut für Experimental Physics, Innsbrück, Austria
7a Tokyo Metropolitain University, Setagaya, Tokyo, Japan
7b Tokyo University of Agriculture and Technology, Koganei, Tokyo, Japan
7c Chuo University, Tokyo, Japan
7d Hiroshima University, Hiroshima, Japan
8 Junta de Energia Nuclear, Madrid, Spain
9 Université de l'Etat à Mons, Mons, Belgium
10 Moscow State University, Moscow, USSR
11 Institute for High Energy Physics, Serpukhov, Protvino, USSR
12 Inst. f. High energy Physics, Vienna, Austria

Submitted to Zeitschrift für Physik C

3601P/PP/ed

ABSTRACT

360 GeV/c proton-proton elastic scattering data obtained at the European Hybrid Spectrometer (EHS) are presented. The differential cross sections of elastic and inelastic pp-interactions are studied as a function of the impact parameter. The results are compared to those obtained at other energies. They are interpreted in the framework of a simple geometrical Monte-Carlo model of inelastic collisions considering protons as composite particles having a definite effective radius with valence quarks inside. The model calculations indicate an increase of the effective radii both of protons and of valence quarks and an increase of the proton opacity with increasing energy. Using this model a description of the overlap function for the total cross section is obtained. A mechanism involving interactions of coloured quarks is proposed leading to a splitting of the overlap function for the total cross section into elastic, inelastic and inelastic diffraction components.

1. INTRODUCTION

Elastic scattering data play an important role in understanding the nature and energy dependence of strong interactions. Using these data one can estimate the size of interacting particles and analyze their internal structure [1]. The shape of angular or momentum-transfer distributions of elastic scattering reflects the wave nature of the colliding particles and the effective radius of their interaction.

It is interesting to consider these interactions in a simple geometrical picture using an impact parameter b, the Fourier transform of the momentum transfer t. The unitarity condition in impact parameter space provides a connection between the total, elastic and inelastic differential cross sections and, consequently, provides an opportunity for studying the properties of inelastic as well as elastic interactions. Using this approach one can draw a number of interesting conclusions concerning the spatial structure of the interaction region and its energy dependence. These conclusions are expressed in the geometrical scaling hypothesis [2], from which it follows that the increase of total cross sections in the ISR energy range reflects the increase with energy of the effective interaction radius.

In the present paper, based upon experimental data for proton-proton elastic scattering at 360 GeV/c (described in sect. 2), we pursue an investigation of the geometrical properties of elastic and inelastic interactions as functions of the impact parameter (sect. 3). The energy range of our experiment is covered by similar investigations done at FNAL and at ISR energies for pp-interactions, whose data we use for comparison. A simplified geometrical picture of inelastic interactions taking into account the quark structure of interacting particles is described in sect. 4. The approximation of the total cross section with our geometrical model and a tentative interpretation of the results in a framework of a model with coloured quarks are described in sect. 5. Conclusions are presented in sect. 6.

2. EXPERIMENTAL APPARATUS AND DATA ANALYSIS

The data used in the present analysis were collected with the Rapid Cycling Hydrogen Bubble Chamber (RCBC) coupled with a wide aperture multi-

particle spectrometer EHS exposed to a proton beam of 360 GeV/c momentum. A detailed description of the experimental procedure has been published [3].

A sketch of the trigger system used in this experiment is presented in fig. 1. An event was recorded if the following trigger condition was satisfied

$$\text{BEAM} * ([\text{ITH} \geq 2] \text{ or } [\text{ITV} \geq 1 \text{ and } \overline{\text{ITV(2)}}]) \quad \text{with}$$

$$\text{BEAM} = T_1 * T_2 * (\overline{V_1 + V_2})$$

where ITH and ITV are the interaction trigger hodoscopes lying in horizontal and vertical planes respectively. ITH includes 26 horizontal counters and ITV consists of 3 vertical fingers. The central finger was narrow horizontally (6 mm) and extended over 25 cm vertically. The beam focus was adjusted to coincide with the vertical axis of ITV(2) the central ITV finger.

Elastic events were selected by cuts on the missing mass squared MM^2 to the event and on the difference $\Delta\theta$ between the measured angle of the fast track and its value calculated from the measured momentum of the slow track assuming an elastic collision. The cuts $|\Delta\theta| \leq 0.6$ mrad and $|MM^2| \leq 0.1\ (GeV/c^2)^2$ were used. Thus we selected 2025 elastic events from the total sample of ~ 4000 two-prong events.

Due to the shape of ITV(2) elastic events having a projectile deflected vertically are lost. This effect is clearly present in the $dN/d\phi$ distribution for slow tracks from elastic events (fig. 2). Here $\phi = \arccos[p_z/(p_y^2 + p_z^2)^{1/2}]$ is the azimuthal angle where p_y and p_z are the orthogonal projections of the recoil transverse momentum with the Y-axis along ITV(2). The losses are concentrated around $\phi = \pi/2$ and $\phi = 3/2\ \pi$. In fig. 3 we show a scatter plot of the azimuthal angles for the fast and slow tracks (for this plot the fast track is rotated by an angle $\phi = \pi$ around the beam axis). Events are clearly concentrated along the line $\phi_{fast} = \phi_{slow}$. The regions affected by the trigger inefficiency are strongly depopulated. Events contributing to these regions were excluded from further analysis. The data presented below correspond to a sample of 1825 elastic events having an azimuthal angle of the slow track within the limits:

$0 \leq \phi \leq 1.0$, $2.0 \leq \phi \leq 4.4$ and $5.2 \leq \phi \leq 2\pi$ rad.

The differential cross section $d\sigma/dt$ for pp elastic scattering at 360 GeV/c as measured in our experiment is presented in fig. 4. The combined effect of the trigger and scan losses is evident at small $|t|$ values: $|t| \leq 0.05$ $(GeV/c)^2$. To avoid $|t|$-dependent corrections only the data with $|t| > 0.05$ $(GeV/c)^2$ were used in the fit.

We fitted our data for the elastic differential cross section with an exponential of the form $A * \exp(Bt + Ct^2)$ treating the optical point value as an ordinary data point. The input parameters for the calculation of the optical point are the total cross section $\sigma_{tot} = (39.8 \pm 0.5)$ mb obtained by interpolation [3] and the ratio of the real to imaginary parts of the elastic amplitude $\rho(s,0) = 0.025 \pm 0.015$, as determined from measurements of pp elastic scattering in the Coulomb nuclear interference region [4]. The results of the fit are given in table 1 together with the results of similar fits for $\sqrt{s} = 23$ GeV and $\sqrt{s} = 31$ GeV data [5]. The corresponding elastic cross section calculated for this experiment is equal to $\sigma_{el} = (6.7 \pm 0.4)$ mb.

3. IMPACT PARAMETER REPRESENTATION

The elastic scattering amplitude in the impact parameter representation $h_{el}(s,b)$ is usually defined as a Fourier transform of the standard elastic scattering amplitude $T_{el}(s,t)$. In the limit of negligible spin effects the following relation can be used [6]:

$$h_{el}(s,b) = \int T_{el}(s,t) J_o(b\sqrt{-t})\, dt/4\pi, \qquad (1)$$

where b is the impact parameter, $J_o(b\sqrt{-t})$ is a zeroth order Bessel function and the amplitude $T_{el}(s,t)$ is related to the observable differential cross section via the relation:

$$\frac{d\sigma_{el}}{dt} = \frac{1}{4\pi} |T_{el}(s,t)|^2 \quad . \qquad (2)$$

The asymptotic s-channel unitarity relation expressed in impact parameter space [7-8] has the functional form (accurate to terms of order 1/s)

$$2\mathrm{Im}\, h_{el}(s,b) = |h_{el}(s,b)|^2 + G_{in}(s,b) \quad . \qquad (3)$$

Then the total, elastic and inelastic differential cross sections in impact parameter space (overlap functions) will have the form:

$$\frac{d\sigma_{tot}}{\pi db^2} = 2Imh_{el}(s,b) = G_{tot}(s,b),$$

$$\frac{d\sigma_{el}}{\pi db^2} = |h_{el}(s,b)|^2 = G_{el}(s,b) \qquad (4)$$

and

$$\frac{d\sigma_{in}}{\pi db^2} = G_{in}(s,b).$$

For the purpose of this work we used a numerical approach as described in [9]. The ratio $\rho(s,t)$ of the real to the imaginary part of the elastic amplitude which is an essential ingredient of this approach, was parametrized according to

$$\frac{1}{\rho(s,t)} = \frac{1}{\rho(s,0)} \left(1 - \frac{|t|}{t_o}\right), \qquad (5)$$

where $t_o = 1.4\ (GeV/c)^2$ corresponds to the position of the first dip in the differential elastic cross section at 360 GeV/c.

Since the impact parameter representation of the elastic amplitude is obtained by integrating over all t-values we must take into account the absence of data for $|t| < 0.05(GeV/c)^2$ and $|t| > 0.6\ (GeV/c)^2$ in this experiment.

To take into account the $|t|$ regions outside the range $0.05 \leq |t| \leq 0.6\ (GeV/c)^2$, we have extrapolated the $d\sigma_{el}/dt$ distribution to $t = 0\ (GeV/c)^2$ using a quadratic exponential as described above and to the value $|t| = 3\ (GeV/c)^2$ using the experimental value of the slope defined in the region $0.4 \leq |t| \leq 0.6\ (GeV/c)^2$ with a single exponential fit. However it is well known that there is a dip at about $|t| \sim 1.4\ (GeV/c)^2$ followed by a secondary maximum; consequently the use of the above procedure may give rise to systematic errors. To estimate the size of these errors we have analyzed data at $\sqrt{s} = 31$ GeV (table 2) in two different ways:

(1) Using the experimental data in the whole experimental t-interval ($0.06 \leq |t| \leq 1.755$ $(GeV/c)^2$ and extrapolating to $t = 0$ $(GeV/c)^2$ with a quadratic exponent and to $|t| = 3 (GeV/c)^2$ by approximating the data above the second maximum ($|t| \sim 1.8$ $(GeV/c)^2$)) with a single exponential form whose slope was taken to be equal to $b = 1.9$ $(GeV/c)^2$ [1(b)].

(2) Using only the interval $0.06 \leq |t| \leq 0.56$ $(GeV/c)^2$ and extrapolating to $t = 0$ $(GeV/c)^2$ and $|t| = 3$ $(GeV/c)^2$ as was done for the present experiment.

Then we have calculated the differences $\Delta G_{21} = G_2 - G_1$ for elastic and inelastic overlap functions, where G_1 and G_2 were obtained by procedures (1) and (2) respectively. The ratios $\Delta G_{21}/G_1$ as functions of the impact parameter b are shown in fig. 5(a) (inelastic) and 5(b) (elastic). We see from fig. 5(a) that the systematic error for the inelastic overlap function is not more than 1% in the region $0 \leq b \leq 1.0$ fm. The systematic error for the elastic overlap function is larger (fig. 5(b)).

In fig. 6 we present the total, elastic and inelastic overlap functions versus the impact parameter b calculated for this experiment. The upper limit of the overlap function for inelastic diffraction is also shown in the figure. This upper limit is known as the Pumplin bound [10] and corresponds to the condition:

$$G_{diff}(b) \leq G_{tot}(b)/2 - G_{el}(b) = G^{max}_{diff}(b). \qquad (6)$$

In comparison with the elastic and total inelastic overlap functions, the upper bound for inelastic diffraction exhibits a more peripheral behaviour, having a maximum around $b \sim 0.6$ fm. Let us recall that the experimentally measured inelastic diffraction cross sections satisfy the following conditions [11]:

$$\sigma_{SD} = (0.68 \pm 0.05) * [1 + (36 \pm 8)/s] * \ln(0.6 + 0.1\ s)\ mb \qquad (7)$$

and

$$\sigma_{DD} = 4/3\ \sigma^2_{SD}/\sigma_{el}\ mb. \qquad (8)$$

Using these expressions we calculated the single and double diffraction cross sections for the energy of this experiment. We found: σ_{SD} = (6.1 ± 0.5) mb and σ_{DD} = (1.7 ± 0.3) mb. Thus the total diffraction cross section amounts to σ_{diff} = (7.8 ± 0.6) mb compared to σ_{diff}^{max} ~ 13.4 mb.

Let us now consider the energy dependence of the overlap functions. In fig. 7(a) we show the difference $\Delta G_{in}(b) = G_{in}(s_1,b) - G_{in}(s_2,b)$ versus b, where $\sqrt{s_1}$ = 53 GeV and $\sqrt{s_2}$ = 26 GeV (this experiment). The input information for $\sqrt{s_1}$ = 53 GeV data is taken from [5] and is listed in table 2. We see from fig. 7(a) that $\Delta G_{in}(b)$ reaches its maximum value around b ~ 1 fm. At b = 0 fm the overlap function is approximately constant, in agreement with ISR data [1]. Thus the increase of the inelastic cross section comes mainly from peripheral inelastic collisions.

In fig. 7(b) we present the distribution of $\Delta G_{el}(b) = G_{el}(s_1,b) - G_{el}(s_2,b)$ which is peaked around b ~ 0.75 fm. This indicates that the increase of the elastic cross section with energy comes from a region which is more central than for the case of the inelastic cross section.

It was already noted [12] that the overlap functions $G_{el}(s,b)$ and $G_{in}(s,b)$ have a kind of Gaussian shape. For the elastic overlap function, this is expected from the Fourier transformation of the approximately exponential behaviour of the elastic $d\sigma_{el}/dt$ differential cross section. However, the complicated shape of the overlap functions measured at different energies shows that both $G_{in}(s,b)$ and $G_{el}(s,b)$ are not purely Gaussian. Following [12] we fitted $G_{el}(s,b)$ and $G_{in}(s,b)$ with a sum of a Gaussian and a so-called "edge" function:

$$d\sigma/\pi db^2 = G_{Gauss} + G_{edge} = A_1 \exp(-b^2/R_1^2) + A_2 b^2 \exp(-b^2/R_2^2). \quad (9)$$

The results of fits for our data are presented in table 3 together with the results of fits of the overlap functions for pp-interactions in the range $\sqrt{s}$ = 9.8-62 GeV and for $\bar{p}p$ interactions at $\sqrt{s}$ = 546 GeV. For this purpose we used information on the differential elastic cross sections the values of the total and elastic cross sections and the values of $\rho(s,t=0)$ (table 2) taken from [5]. It is seen from table 3 that for the inelastic overlap function the contribution of G_{edge} decreases with

increasing energy and has a tendency to flatten in the ISR energy range. For the elastic overlap function the fraction of G_{edge} is approximately constant for the whole energy range up to the highest ISR energies. At $\sqrt{s}$ = 546 GeV the contribution of G_{edge} increases significantly for the inelastic overlap function. It has been shown [8] that the difference ΔG_{in} (b) between $\bar{p}p$ and pp at $\sqrt{s}$ = 53 GeV is small (less than 2%). The significant increase of G_{edge} at $\sqrt{s}$ = 546 GeV cannot therefore be explained by the difference of G_{in} (b) between $\bar{p}p$ and pp interactions. For the elastic overlap function, it is comparable, within two standard deviations, with those in the ISR energy range.

The s-dependence of the overlap function and of the elastic and inelastic cross sections is closely related to the energy dependence of the mean effective interaction radius squared which is calculated as follows:

$$\langle r^2 \rangle = \int_o^{b_{max}} b^2 G(b)\, bdb / \int_o^{b_{max}} G(b) bdb \quad . \tag{10}$$

The value of $R \equiv \sqrt{\langle r^2 \rangle}$ will depend on the choice of b_{max}, but it should flatten at large b_{max} values. In figs 8(a,b) we show values of R as a function of b_{max} for elastic and inelastic interactions calculated for our data and for data at $\sqrt{s}$ = 53 GeV. At $\sqrt{s}$ = 26 GeV the value R_{el} reaches a plateau R_{el} = (0.63 ± 0.01) fm at $b_{max} \sim 1.8$ fm (fig. 8(a)). The plateau at $\sqrt{s}$ = 53 GeV is reached at $b_{max} \sim 2.0$ fm and is equal to R = (0.662 ± 0.003)fm. For inelastic interactions the value R_{in} is increasing with b_{max} up to the highest values of b ~ 2.4 fm for which data are available. At b_{max} = 2.4 fm we have obtained the lower estimates R_{in} = (1.033 ± 0.020) fm ($\sqrt{s}$ = 26 GeV) and R_{in} = (1.048 ± 0.005) fm ($\sqrt{s}$ = 53 GeV).

Using the results of the fits of the inelastic and elastic overlap functions we calculated R with $b_{max} = \infty$. The results of our calculations are presented in table 3. We see from this table that the effective interaction radius is increasing with energy for both inelastic and elastic interactions. The results clearly indicate that elastic interactions are more central in impact parameter representation than inelastic ones.

4. A SIMPLE GEOMETRICAL MODEL OF INELASTIC HADRON-HADRON INTERACTIONS

It is a well-known experimental fact that in head-on collisions the probability of inelastic interactions is less than the unitarity limit $G_{in}^{lim}(b = 0) = 1$ which corresponds to the collision of two absolutely opaque discs. This means that protons are grey and have a non-zero probability $1 - G_{in}(s,b = 0) \sim 0.06$ (which is usually called transparency) to pass each other without interacting. The same observation is valid for πp and Kp inelastic interactions in which the transparency is of the order of ~ 0.18 and ~ 0.25 respectively [13].

The difference of the transparency in pp, πp and Kp interactions can be connected with the number of valence quarks inside hadrons as well as with their effective size. Following this idea we considered a simple "geometrical" Monte-Carlo model (GM) of inelastic hadron-hadron collisions. A schematic drawing of this model for pp interactions is given in fig. 9. Here b is the impact parameter for protons and d is the one for a pair of dressed quarks called valons. The condition for an inelastic interaction in such a picture is $d_{ij} \leq 2r_v$ for at least one pair of valons i and j from different protons. Thus the model contains two parameters only: the effective radius of the hadron r_h and of the valon r_v. The position of valons inside a proton $\vec{R}_v$ is generated randomly according to the following conditions:

$$\begin{aligned} &|\vec{R}_{v_i} - \vec{R}_{v_j}| \geq 2r_v \quad \text{and} \\ &|\vec{R}_v| \leq r_h - r_v \quad , \end{aligned} \tag{11}$$

with the zero of the coordinate system at the centre of the hadron.

In fig. 10(a) we present the results of our Monte-Carlo parametrization (solid line) for the inelastic overlap function calculated in this experiment. Radii of the proton and valons are determined by minimizing:

$$\chi^2 = \sum_{i=1}^{11} |G_{in}^{exp}(b_i) - G_{in}^{GM}(b_i)|^2/(\Delta G_{in}^{exp}(b_i))^2 \tag{12}$$

giving the values: $r_p = (0.98 \pm 0.03)$ fm and $r_v = (0.203 \pm 0.003)$ fm (table 4) in the interval b = 0–1 fm. It is seen from fig. 10(a) that GM reproduces well the experimental values of $G_{in}(b)$ up to $b \sim 1.2$ fm.

If one assumes that the increase of the interaction radius with energy is due to an increase of the size of both the proton and valon then one can estimate the energy dependence of their radii in the framework of GM. We used for this purpose the experimental data for pp interactions at c.m.s. energies equal to $\sqrt{s}$ = 9.78 GeV (p_{lab} = 50 GeV/c), 13.8 GeV (p_{lab} = 100 GeV/c), 19.4 GeV (p_{lab} = 200 GeV/c), 23, 31, 53 and 62 GeV together with data for $p\bar{p}$ interactions at $\sqrt{s}$ = 546 GeV [5]. The effective radii of proton (antiproton) and of valons in inelastic collisions were estimated in the same way as for this experiment and the results are presented in table 4. The value δ in this table corresponds to

$$\delta = \sum_{i=1}^{11} |G_{in}^{exp}(b_i) - G_{in}^{GM}(b_i)| \Sigma\, G_{in}^{exp}(b_i) \ . \qquad (13)$$

We note that for each energy an extrapolation into the |t| region below the experimental limit is done with a quadratic exponential form using the optical point value as a data point. The extrapolation into the |t| region above the experimental limit (up to |t| = 3 $(GeV/c)^2$) is done with a single exponential form with b = 1.9 $(GeV/c)^2$.

A fit of the form $r = A + B\ln(s/s_o)$ (s_o = 1 GeV^2) to the combined pp and $\bar{p}p$ data in the energy interval $\sqrt{s}$ = 23 - 546 GeV yields the results A_p = (0.86 ± 0.04) fm, B_p = (0.024 ± 0.005) fm and A_v = (0.142 ± 0.005) fm, B_v = (0.0093 ± 0.0006) fm for r_p and r_v, respectively (fig. 11).

It is evident that the resulting r_p and r_v values depend on the relative distribution of the valons inside the proton. Therefore we also considered the case when two valons are combined in a di-valon configuration. This is done with the condition $|\vec{R}_{v_1} - \vec{R}_{v_2}| = 2r_v$. The results are presented in table 4, and we find for the s-dependence of r_p and r_v: A_p^{di} = (0.857 ± 0.042) fm, B_p^{di} = (0.029 ± 0.005) fm and A_v^{di} = (0.172 ± 0.005) fm, B_v^{di} = (0.010 ± 0.001) fm respectively.

Both the fits of r_p and r_v for free valons and di-valon configurations give approximately the same shapes of energy dependences: $B_{p(v)}$(free valons) ~ $B_{p(v)}$ (di-valon).

Using the previous results we estimated the "density" of valons inside the proton by simply calculating the ratio $3r_v^3/r_p^3$ which reflects the opacity of the proton (antiproton) in inelastic collisions. In the energy range $\sqrt{s}$ = 23–546 GeV this ratio increases by 1.43 ± 0.20 and 1.26 ± 0.20 for the free valons and di-valon configurations respectively. Thus in the framework of these two pictures the conclusion can be drawn that there is some indication for an increase of the proton (antiproton) opacity with increasing energy.

In fig. 7(a), where the difference $\Delta G_{in}(b)$ between $\sqrt{s}$ = 53 GeV and $\sqrt{s}$ = 26 GeV is presented, the solid line shows the prediction of GM with independent valons. The agreement with experimental data is good. Thus the increase of the peripheral inelastic pp cross section with increasing energy can be interpreted as a reflection of the increase of the radii of the protons and valons.

The transition from pp to πp inelastic collisions is rather simple in the framework of the GM model: the number of valons in a π-meson is taken equal to two and the values of r_v^π and r_π can be obtained in a similar way as for pp interactions. As an example we show in fig. 10(b) the results of such a fit for π^+p interactions at p_{lab} = 200 GeV/c [14]. The total and elastic cross sections we take to be σ_{tot} = (23.78 ± 0.04) mb, σ_{el} = (3.17 ± 0.06) mb with $\rho(t = 0) = 0.05 \pm 0.06$. The experimental values of the elastic differential cross section $d\sigma_{el}/dt$ were taken in the interval $0.08 \leq |t| \leq 1.35$ (GeV/c)^2. The extrapolation to t = 0 (GeV/c)^2 is done with a quadratic exponential form and to t = 3 (GeV/c)^2 with a single exponential form as defined in the region $0.8 \leq |t| \leq 1.35$ (GeV/c)^2. We used in the fit the values of r_p and r_v^p for a configuration of free valons from table 4 for an incident momentum of p_{lab} = 200 GeV/c ($\sqrt{s}$ = 19.4 GeV). The fit yields: r_π = (0.74 ± 0.06) fm and r_v^π = (0.16 ± 0.01) fm.

5. THE GEOMETRICAL MODEL WITH COLOURED QUARKS

In the previous chapter there are two motivations for using our geometrical model for the description of the inelastic overlap function G_{in}. The first one is that the unitarity limit $G_{in}(s,b=0) = 1$ provides an

absolute normalization of G_{in} at a given energy. With respect to the value $G_{in}^{lim}(s,b=0) = 1$ the experimental value $G_{in}^{exp}(s,b=0)$ can be considered simply as the probability for valons to have at least one interaction for a head-on collision. The second motivation is that the increase of the total cross section at moderate energies is mainly due to the increase of the inelastic cross section.

Within the GM framework it is interesting to consider the overlap function corresponding to the total cross section. Neglecting the real part of the elastic amplitude we can rewrite the expressions for G_{tot} and G_{el} as (eqs (3) and (4)):

$$G_{tot}(s,b) = 2[1 - \sqrt{1 - G_{in}(s,b)}]$$
$$G_{el}(s,b) = [1 - \sqrt{1 - G_{in}(s,b)}]^2 \qquad (11)$$

It follows that if the unitarity limit is satisfied for G_{in}, then $G_{el}^{lim}(s,b=0) = 1$ and $G_{tot}^{lim}(s,b=0) = 2$. This is the black disk limit for which $\sigma_{el}^{lim}/\sigma_{tot}^{lim} = 0.5$. We obtain for the proton opacity in head-on hadronic collisions $G_{tot}(s,b=0) = 0.75$ at $\sqrt{s} = 26$ GeV.

Now we can use GM to approximate $G_{tot}(b)$ in the same way as was done for the inelastic overlap function. This approximation is shown in fig. 12 (solid curve) with values $r_p = 0.91$ fm and $r_v = 0.14$ fm.

In an attempt to split the overlap function for the total cross section into inelastic, elastic and inelastic diffractive components, we consider in a first step one gluon exchange between coloured valence quarks. With this assumption if a collision of two valons containing valence quarks of different colours (red and blue for example) occurs then: q_1(red) + q_2(blue) → q_1(blue) + q_2(red). Then we assume: if after all the collisions of valons which occurred during the hadron interaction these hadrons remain neutral in colour this interaction must be considered to be elastic or inelastic diffraction. If this is not the case then such a collision must be considered to be purely inelastic (without inelastic diffraction). In the last case the colour string should be stretched between coloured hadrons initiating a hadronization process.

If only one pair of valons is involved in the collision we assume that it leads to an inelastic interaction. The reason for this is the more central shape of the elastic overlap function in comparison to the inelastic one (fig. 6) and thus the difference $G_{in}(b) - G_{el}(b)$ has a peripheral shape which is compatible with the shape of single collisions of valons. As is seen from fig. 6 the Pumplin limit for inelastic diffraction has a peripheral shape too. We therefore expect that inelastic diffraction comes mainly from single collision of valons.

To summarize, to split $G_{tot}(b)$ into elastic, inelastic and inelastic diffraction components we define:

- Elastic collisions: multiple collisions of valons (more than 1 hit) after which protons remain colourless;
- Inelastic diffraction: single collision of valons after which protons remain colourless;
- Purely inelastic: Collisions after which protons are coloured.

Introducing these criteria in GM we find that the elastic and diffractive cross sections at the energy of this experiment are lower than the experimental values. Therefore if $d_{vv} \leq .250$ fm (here d_{vv} is the impact parameter for valons) double gluon exchange is introduced. It leads to a good approximation of $G_{el}(b)$ (fig. 12). To reproduce the experimental ratio $\sigma_{diff}/\sigma_{in} = 0.24$, we attribute to diffraction the peripheral single collision of valons with $d_{vv} \geq .215$ fm. The resulting profile of $G_{diff}(b)$ is shown in fig. 12. Note that a purely inelastic interaction will now include single collision of valons with $d_{vv} < .215$ fm, the protons remaining colourless.

This simple Geometrical Model reproduces well:

- The experimentally observed increase of σ_{el}/σ_{tot} from ISR to collider energies.
- The experimentally observed increase of σ_{diff} at ISR.

The predictions of GM for the total cross section for the 2-40 TeV region are in agreement with theoretical predictions of C. Bourrely and A. Martin [15].

6. CONCLUSIONS

(a) We have presented experimental data on pp elastic scattering at 360 GeV/c in the t-region $0.05 \leq |t| \leq 0.6$ $(GeV/c)^2$. The differential cross section $d\sigma/dt$ was parametrized by the quadratic exponential form $A \exp(Bt + Ct^2)$ using the optical point value as a data point. The results of the fit are: $A = (80.9 \pm 1.9)(mb/(GeV/c)^2)$, $B = (13.2 \pm 0.5)(GeV/c)^{-2}$ and $C = (6.9 \pm 1.3)(GeV/c)^{-4}$. The corresponding elastic cross section is equal to $\sigma = (6.7 \pm 0.4)$ mb.

(b) The results of an impact parameter analysis of our data are in agreement with those published in the FNAL-ISR energy range and can be summarized as follows:

- Both the elastic and inelastic overlap functions $G_{el}(b)$ and $G_{in}(b)$ have a maximum at the value b = 0 fm of impact parameter.
- The effective interaction radii R for inelastic and elastic interactions increase with increasing energy. R for inelastic interactions is approximately 1.5 R for elastic ones.
- The profile of the upper limit for inelastic diffraction $G^{max}_{diff}(b)$ has a peripheral behaviour. The total diffractive cross section from the parametrization (7) and (8) is approximately 1.7 times smaller than the Pumpling bound.

(c) A simple geometrical Monte-Carlo model (GM) was proposed for inelastic collisions based on the assumption that the value of the transparency $1 - G_{in}(b = 0)$ in head-on collisions of hadrons reflects the number of valence quarks inside hadrons and the effective ("inelastic") radii of both hadrons and quarks. From comparisons of the model predictions with data for pp and πp interactions the following conclusions can be drawn:

- Assuming independent valons inside the proton the profile of the inelastic overlap functions in pp and πp interactions is reproduced up to impact parameter values b ~ 1.2 fm and b ~ 1 fm respectively.
- At the energy of this experiment the effective radii of proton and valons are equal to $r_p = (0.98 \pm 0.03)$ fm and $r_v^p = (0.203 \pm 0.003)$ fm.
- In π^+p interactions at $p_{lab} = 200$ GeV/c the effective radii of pion and valons inside the pion are $r_\pi = (0.74 \pm 0.06)$ fm and $r_v^\pi = (0.160 \pm 0.01)$ fm.

- The effective radii of proton and valons in $pp(\bar{p})$ inelastic collisions increase logarithmically in the energy interval $\sqrt{s} \sim 20 - 546$ GeV.

- For $pp(\bar{p})$ inelastic collisions a similar conclusion is also valid for a di-valon configuration inside the proton ($|\vec{R}_{v_1} - \vec{R}_{v_2}| = 2r_v$). For such a configuration the values of r_p and r_v are systematically higher than the ones obtained in the case of the independent valons.

- For both configurations one finds indications for an increase of the proton opacity with increasing energy.

- A simplified interaction mechanism was proposed: The overlap function for the total cross section was approximated with GM, and coloured valence quark collisions were considered. Within this framework the overlap function could be decomposed into elastic, inelastic and inelastic diffractive components. With the specific criteria which are described in sect. 5 we obtained a good approximation of the elastic, inelastic and inelastic diffractive cross sections measured and calculated (for inelastic diffraction) in this experiment.

REFERENCES

[1] (a) U. Amaldi and K.R. Schubert, Nucl. Phys. B166 (1980) 301;
(b) G. Alberi and G. Goggi, Phys. Rep. 74 (1981) 1;
(c) M. Kamran, Phys. Rep. 108 (1984) 275;
(d) R. Castaldi and G. Sanguinetti, Ann. Rev. Nucl. Part. Sci. 35 (1985) 351.

[2] J. Dias de Deus, Nucl. Phys. B59 (1973) 231;
A.J. Buras and J. Dias de Deus, Nucl. Phys. B71 (1974) 481;
R. Henzi and P. Valin, Phys. Lett. 132B (1983) 443.

[3] J.L. Bailly et al., Z. Phys. C23 (1984) 205.

[4] V. Bartenev et al., Phys. Rev. Lett. 31 (1973) 1367.

[5] V.V. Ezhela, Comp. Phys. Com. 33 (1984) 225.

[6] V.L. Savrin et al., Soviet Journal of Nuclear Physics V10 (1969) 495 (transl.).

[7] U. Amaldi, M. Jacob and G. Matthiae, Ann. Rev. Nucl. Sc. 26 (1976) 385.

[8] T. Fearnly, CERN/EP 85-137.

[9] M.I. Bogoljubski et al., Sov. Journal of Nucl. Phys. V33 (1981) 66 (transl.).

[10] J. Pumplin, Phys. Rev. D8 (1973) 2899.

[11] K. Goulianos, Phys. Rep. 101 (1983) 171.

[12] R. Henzi and P. Valin, Phys. Lett. 48B (1974) 119.

[13] D.S. Ayres et al., Phys. Rev. D14 (1976) 3092.

[14] A. Shiz et al., Phys. Rev. D4 (1981) 26.

[15] C. Bourrely and A. Martin, CERN TH 3931.

TABLE CAPTIONS

TABLE 1 The results of the fits of the quadratic exponential form $A \exp(Bt + Ct^2)$ to the $d\sigma/dt$ distribution, for this experiment and for $\sqrt{s}$ = 23 GeV and $\sqrt{s}$ = 31 GeV.

TABLE 2 Input data to the impact parameter representation for pp interactions at various energies and for $p\bar{p}$ interactions at $\sqrt{s}$ = 546 GeV.

TABLE 3 The results of the approximation of elastic and inelastic overlap functions with the expression: $G_{el(in)}(b) = A_1 \exp(-b^2/R_1^2) + A_2 b^2 \exp(-b^2/R_2^2)$. The effective interaction radius R and the ratio $\sigma_{edge}/(\sigma_{Gauss} + \sigma_{edge})$ are also given.

TABLE 4 The results of GM approximation of inelastic overlap functions for pp and $p\bar{p}$ ($\sqrt{s}$ = 546 GeV) interactions for independent valon and di-valon configuration inside the proton. Here $\delta = \Sigma |G_{in}^{exp}(b_i) - G_{in}^{GM}(b_i)| / \Sigma\, G_{in}^{exp}(b_i)$.

TABLE 1

$\sqrt{s}$ (GeV)	$-t$ $(GeV/c)^2$	A $mb/(GeV/c)^2$	Opt. Point $mb/(GeV/c)^2$	B $(GeV/c)^{-2}$	C $(GeV/c)^{-4}$	χ^2/NDF
26	0.05-0.6	80.9 ± 1.9	80.7 ± 2.0	13.19 ± 0.46	6.91 ± 1.31	49/43
31	0.05-0.72	83.0 ± 0.8	82.5 ± 1.0	12.24 ± 0.20	2.23 ± 0.43	17/20
23	0.03-0.775	77.5 ± .7	78.7 ± 3.2	12.28 ± 0.24	2.77 ± 0.55	10.8/28

TABLE 2

$\sqrt{s}$ (GeV)	9.8	13.8	19.4	23	26[a]	31	53	62	546
σ_{tot} (mb)	38.20 ± 0.04	38.5 ± 0.1	39.3 ± 0.1	39.4 ± 0.8	39.8 ± 0.5	40.2 ± 0.2	42.9 ± 0.2	43.9 ± 0.3	61.9 ± 1.5
σ_{el} (mb)	7.46 ± 0.12	7.15 ± 0.20	6.9 ± 0.3	6.7 ± 0.1	6.7 ± 0.4	7.1 ± 0.3	7.6 ± 0.3	7.7 ± 0.2	13.3 ± 0.4
$\rho(s, 0)$	-0.16 ± 0.05	-0.1 ± 0.1	-0.06 ± 0.1	0.02 ± 0.05	0.025 ± 0.015	0.042 ± 0.011	0.078 ± 0.011	0.095 ± 0.011	0.15 ± 0.01
$\lvert t\rvert$ $(GeV/c)^2$	0.075-3.0	0.075-2.8	0.075-3.25	0.03-2.15	0.05-0.6	0.06-1.775	0.105-2.05	0.1-1.775	0.1-1.55

(a) This experiment.

TABLE 3

$\frac{d\sigma}{\pi db^2}$	$\sqrt{s}$ (GeV)	A_1	A_2 (fm^{-2})	R_1 (fm)	R_2 (fm)	χ^2/NDF	R (fm)	$\frac{\sigma_{edge}}{\sigma_G + \sigma_{edge}}$
I	9.8	.930 ± .002	.73 ± .01	0.983 ± .005	.685 ± .008	55/24	.981 ± .004	.151 ± .006
N	13.8	.936 ± .001	.62 ± .01	1.006 ± .004	.683 ± .008	19/24	1.001 ± .004	.125 ± .006
E	19.4	.927 ± .002	.53 ± .02	1.037 ± .005	.682 ± .012	5/24	1.030 ± .005	.103 ± .007
L	23	.914 ± .009	.46 ± .11	1.072 ± .019	.646 ± .068	24/22	1.062 ± .018	.070 ± .032
A	26	.940 ± .008	.59 ± .11	1.064 ± .012	.574 ± .040	6/24	1.051 ± .012	.057 ± .018
S	31	.935 ± .004	.44 ± .04	1.042 ± .018	.751 ± .038	12/21	1.045 ± .017	.122 ± .024
T	53	.925 ± .003	.50 ± .03	1.097 ± .006	.669 ± .016	18/24	1.086 ± .005	.083 ± .008
I	62	.919 ± .002	.49 ± .03	1.127 ± .004	.631 ± .015	21/24	1.114 ± .004	.063 ± .007
C	546	.965 ± .001	.61 ± .01	1.149 ± .012	.861 ± .012	4/24	1.164 ± .010	.209 ± .011
	9.8	.642 ± .006	.22 ± .07	.641 ± .001	.444 ± .026	59/24	.641 ± .002	.031 ± .012
E	13.8	.587 ± .005	.38 ± .10	.657 ± .001	.370 ± .019	95/24	.654 ± .001	.027 ± .009
L	19.4	.537 ± .006	.38 ± .15	.676 ± .002	.353 ± .028	33/22	.673 ± .002	.023 ± .012
A	23	.488 ± .023	.73 ± 1.01	.693 ± .008	.301 ± .101	3/24	.688 ± .012	.025 ± .047
S	26	.548 ± .022	1.33 ± .97	.669 ± .007	.296 ± .050	16/24	.661 ± .009	.040 ± .038
T	31	.544 ± .010	2.49 ± 2.93	.690 ± .003	.162 ± .060	12/21	.688 ± .005	.007 ± .012
I	53	.534 ± .008	.51 ± .21	.704 ± .002	.356 ± .030	52/24	.700 ± .003	.030 ± .015
C	62	.520 ± .007	.90 ± .27	.717 ± .002	.318 ± .022	108/24	.710 ± .003	.033 ± .013
	546	.811 ± .006	.04 ± .05	.763 ± .002	.560 ± .154	7/24	.764 ± .003	.009 ± .015

TABLE 4

	$\sqrt{s}$ (GeV)	9.8	13.8	19.4	23	26[a]	31	53	62	546
	G_{in}^{exp} (b = 0 fm)	.930 ± .002	.935 ± .002	.925 ± .003	.913 ± .013	.941 ± .010	.931 ± .006	.930 ± .004	.920 ± .003	.964 ± .002
	G_{in}^{exp} (b = 1 fm)	.387 ± .003	.391 ± .003	.398 ± .003	.397 ± .019	.386 ± .013	.420 ± .007	.431 ± .004	.432 ± .005	.584 ± .004
free valons	χ^2/11 (0 ≤ b ≤ 1 fm)	3.3	2.6	1.7	0.12	0.18	0.62	0.73	0.71	2.0
	δ (%)	0.05	0.12	0.4	0.13	0.01	0.60	0.40	0.40	0.60
	r_p (fm)	.99 ± .02	.99 ± .02	1.02 ± .02	1.02 ± .02	.98 ± .03	1.03 ± .02	1.05 ± .02	1.07 ± .03	1.16 ± .03
	r_v (fm)	.205 ± .003	.204 ± .002	.204 ± .003	.201 ± .002	.203 ± .003	.209 ± .003	.214 ± .003	.213 ± .003	.261 ± .003
di valons	χ^2/11 (0 ≤ b ≤ 1 fm)	6.7	5.0	0.50	0.34	0.18	0.43	0.68	0.80	4.5
	δ (%) (0 ≤ b ≤ 1 fm)	0.60	0.38	0.22	1.10	0.34	0.10	0.24	0.10	0.23
	r_p (fm)	1.02 ± .03	1.03 ± .02	1.03 ± .02	1.03 ± .02	1.01 ± .03	1.07 ± .02	1.09 ± .02	1.10 ± .03	1.21 ± .03
	r_v (fm)	.234 ± .004	.236 ± .005	.236 ± .005	.232 ± .004	.236 ± .004	.244 ± .003	.248 ± .004	.250 ± .004	.300 ± .007

(a) This experiment.

FIGURE CAPTIONS

Fig. 1 A sketch of the interaction trigger system used in the NA23 experiment.

Fig. 2 The distribution of the azimuthal angle (in the plane orthogonal to the beam direction) of the recoil protons in elastic events.

Fig. 3 Scatter plot of azimuthal angles of fast (Y-axis) and of slow (X-axis) tracks for elastic events (fast tracks are rotated by 180° around the beam direction).

Fig. 4 The differential cross section $d\sigma/dt$ for pp elastic scattering at p_{lab} = 360 GeV/c.

Fig. 5 The ratio $\Delta G_{21}(b)/G_1(b) = [G_2(b) - G_1(b)]/G_1(b)$ at $\sqrt{s}$ = 31 GeV where $G_1(b)$ and $G_2(b)$ are calculated by the two different procedures discussed in the text.

(a) For the inelastic overlap functions;
(b) For the elastic overlap functions.

Fig. 6 The total, elastic and inelastic differential cross sections (overlap functions) and the Pumplin limit for inelastic diffraction in pp interactions at 360 GeV/c as functions of the impact parameter.

Fig. 7 The difference between the overlap functions measured at different energies(black points):

(a) $G_{in}(\sqrt{s} = 53 \text{ GeV}) - G_{in}(\sqrt{s} = 26 \text{ GeV})$;
(b) $G_{el}(\sqrt{s} = 53 \text{ GeV}) - G_{el}(\sqrt{s} = 26 \text{ GeV})$.

The solid line gives the GM predictions.

Fig. 8 The variation of the effective interaction radius R computed for elastic (fig. 8(a)) and inelastic (fig. 8(b)) pp interactions as a function of the integration limit b_{max} for this experiment (black points) and for $\sqrt{s}$ = 53 GeV (p_{lab} = 1480 GeV/c) (crosses).

FIGURE CAPTIONS (Cont'd)

Fig. 9 The geometrical picture of proton-proton inelastic collisions as viewed in the geometrical Monte-Carlo model (GM). Here r_p and r_v^p are the radii of the proton and of the valons and b and d are the impact parameters for proton-proton and valon-valon collisions respectively.

Fig. 10 (a) Comparison of the inelastic overlap function $G_{in}(b)$ with the prediction of the GM model in this experiment.

(b) Comparison of the inelastic overlap function $G_{in}(b)$ with the prediction of the GM model for $\pi^+ p$ interactions at $P_{lab} = 200$ GeV/c.

Fig. 11 The energy dependence of r_v^p and r_p for a configuration with independent valons inside the proton. The straight lines are fits with the expression $r = A + B\ln(s/s_o)$ ($s_o = 1$ Gev^2), where $A_p = (0.860 \pm 0.042)$ fm, $B_p = (0.0240 \pm 0.0005)$ fm and $A_v = (0.142 \pm 0.005)$ fm, $B_v = (0.0093 \pm 0.0006)$ fm.

Fig. 12 Predictions of GM with coloured quarks for the inelastic, elastic and inelastic diffraction overlap functions in comparison with the experimental distributions (this experiment) of elastic and inelastic overlap functions. The GM approximation of the overlap functions for the total cross section is also shown.

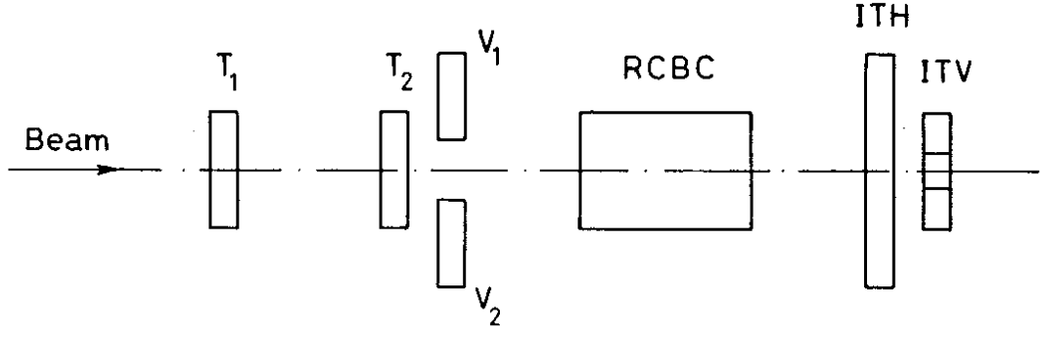

Fig. 1

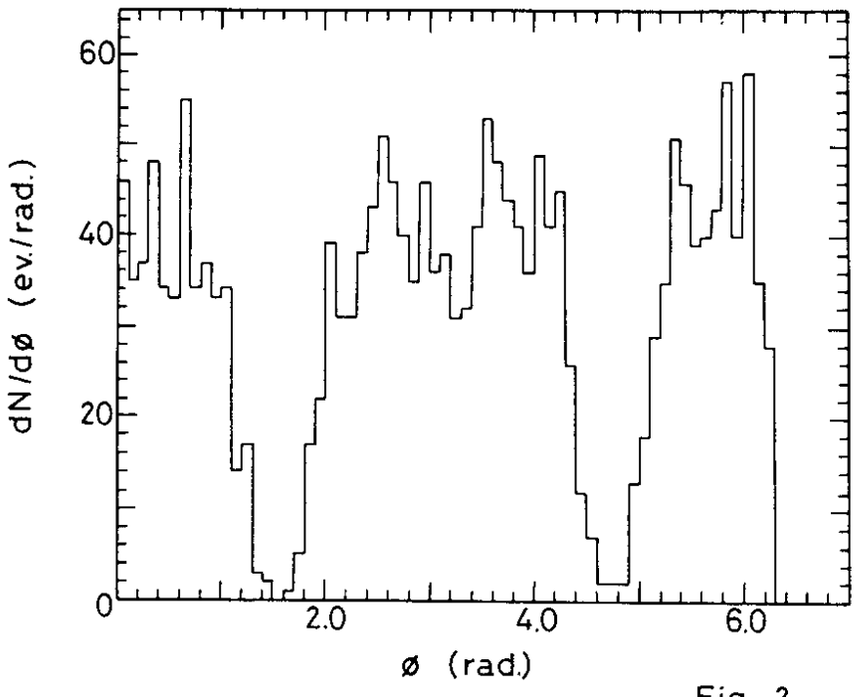
60
40
20
0
dN/dø (ev./rad.)
2.0
4.0
6.0
ø (rad.)

Fig. 2

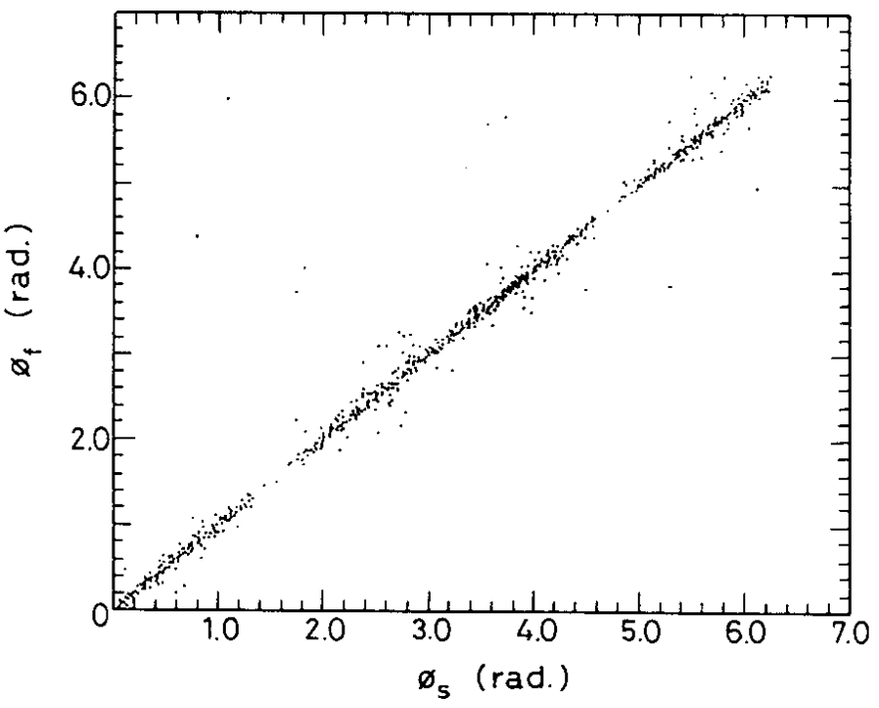
6.0
4.0
2.0
0
ø_f (rad.)
1.0
2.0
3.0
4.0
5.0
6.0
7.0
ø_s (rad.)

Fig. 3

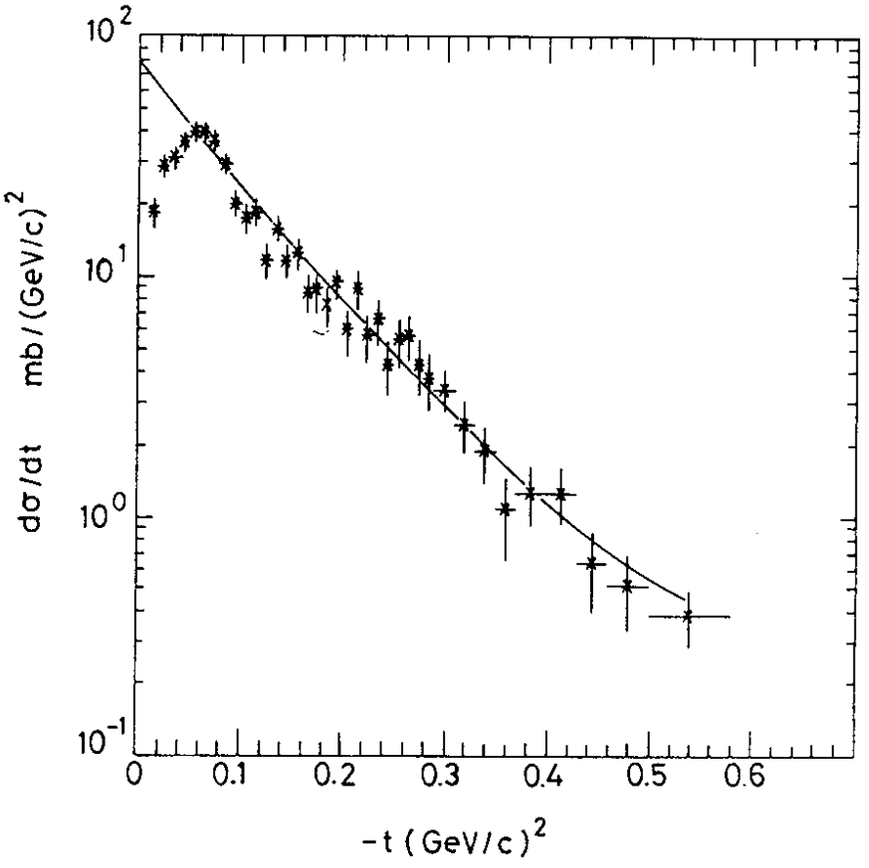

Fig. 4

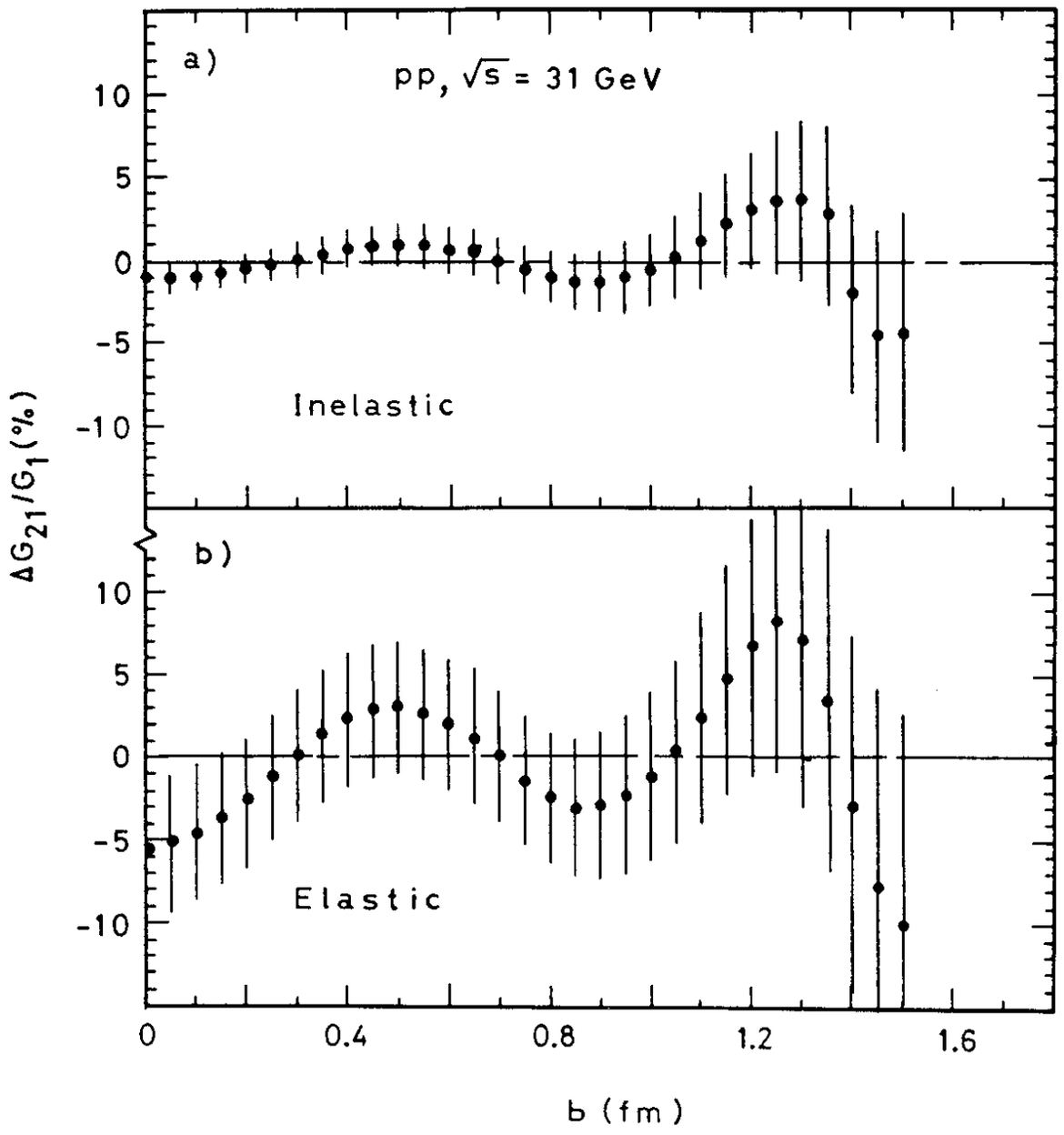
a)
pp, √s = 31 GeV
Inelastic
b)
Elastic
10
5
0
-5
-10
0
0.4
0.8
1.2
1.6
b (fm)
ΔG21/G1(%)

Fig.5

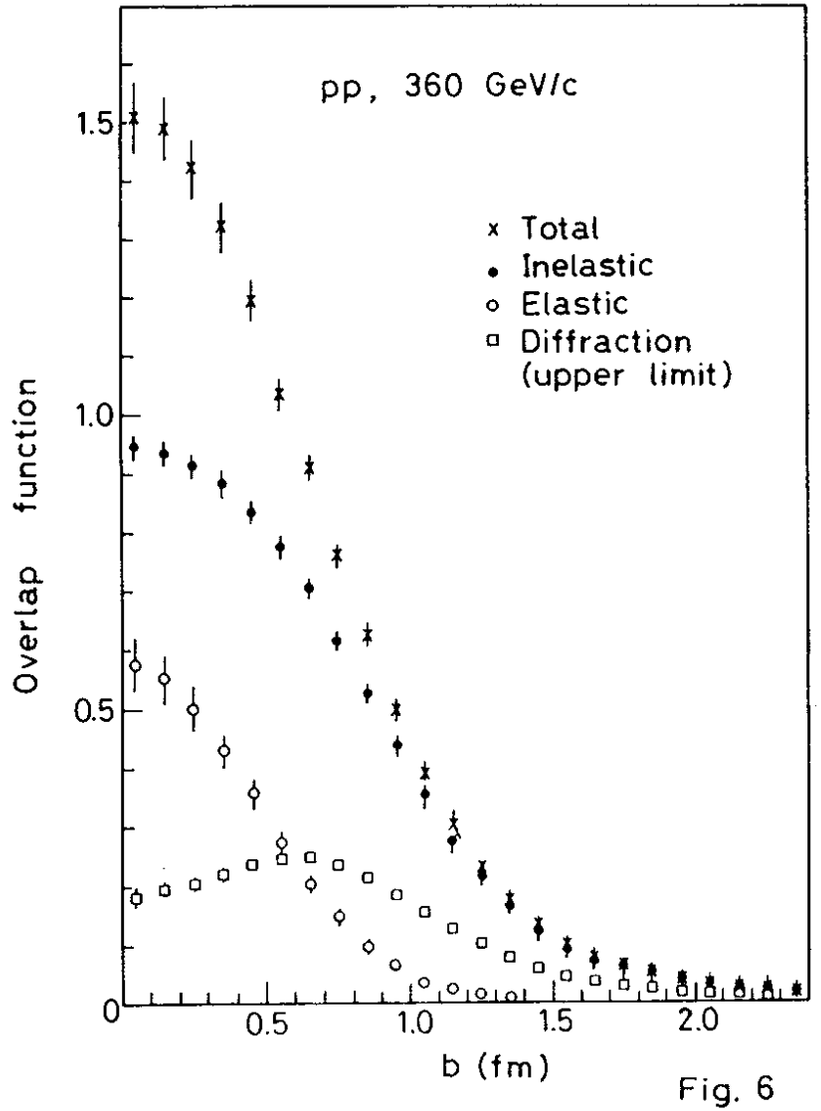
pp, 360 GeV/c
x Total
• Inelastic
o Elastic
□ Diffraction
(upper limit)
Overlap function
1.5
1.0
0.5
0
0.5
1.0
1.5
2.0
b (fm)

Fig. 6

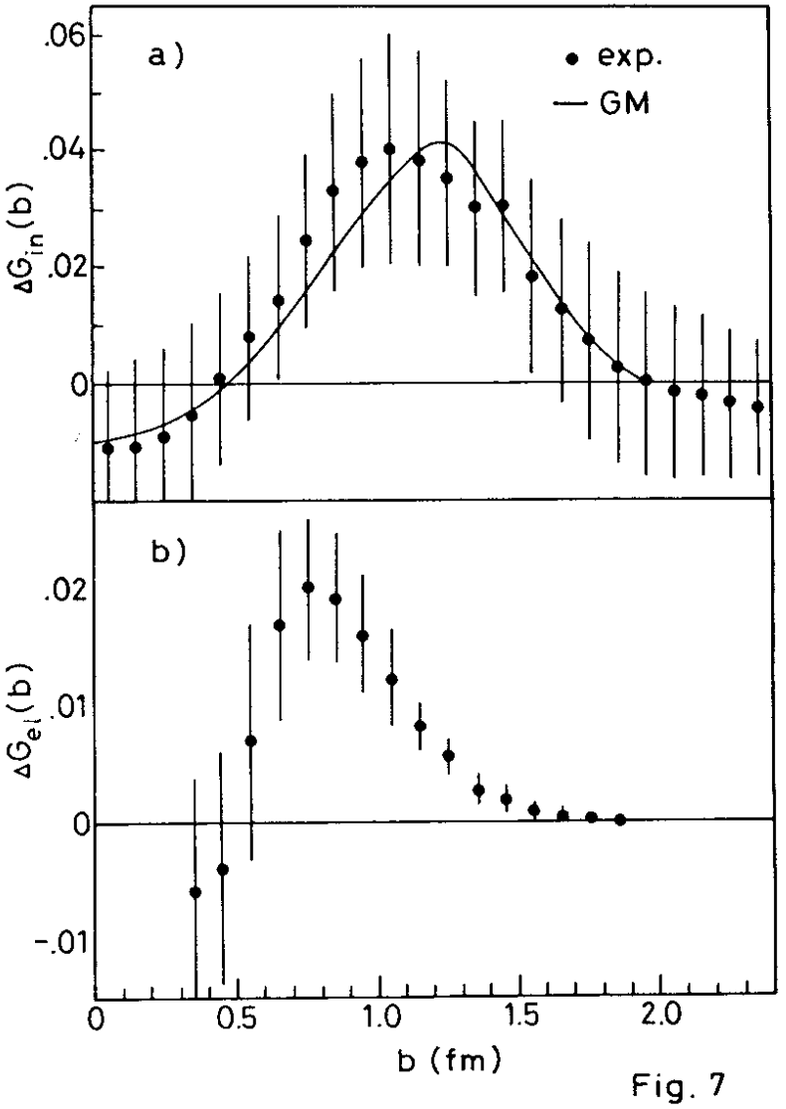
a)
• exp.
— GM
$\Delta G_{in}(b)$
.06
.04
.02
0
b)
$\Delta G_{el}(b)$
.02
.01
0
-.01
0
0.5
1.0
1.5
2.0
b (fm)

Fig. 7

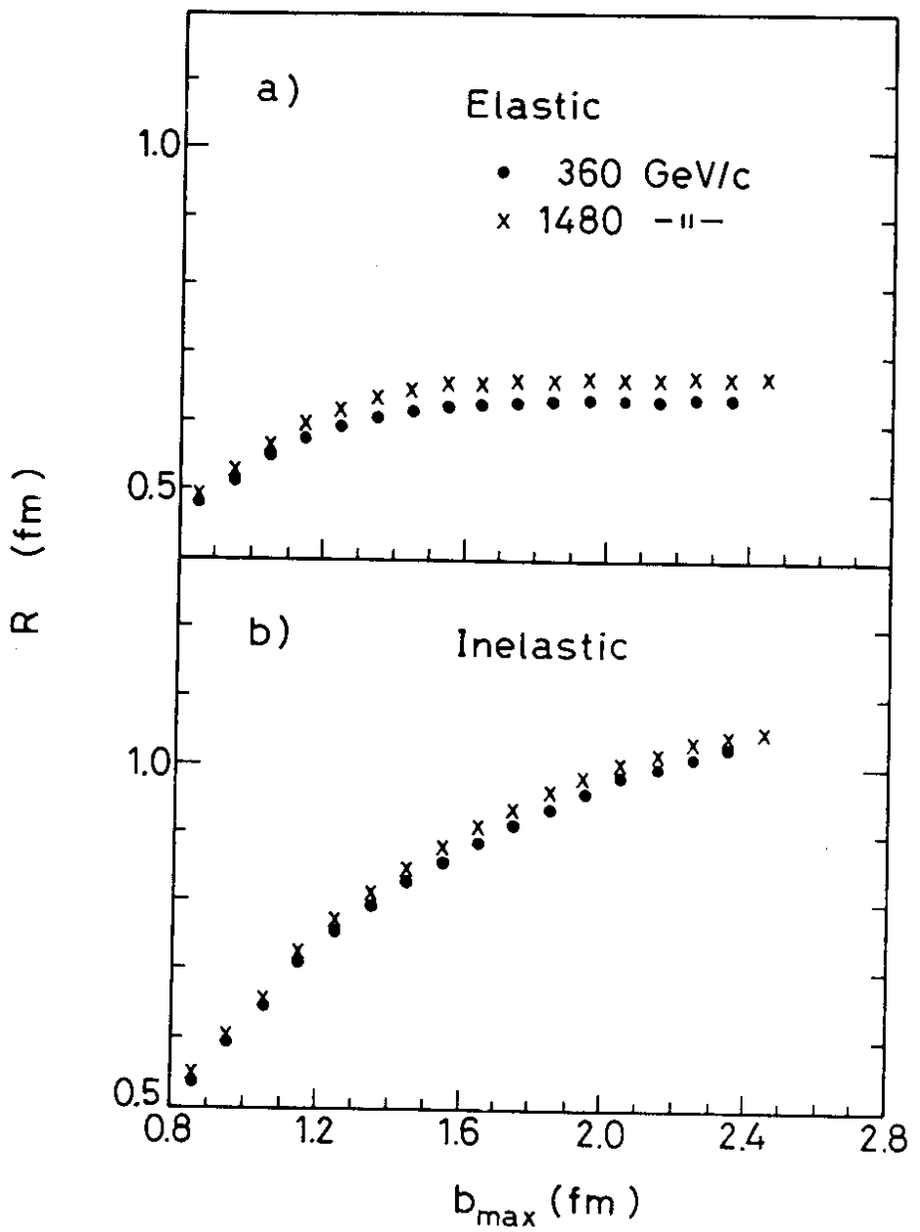
a)
Elastic
• 360 GeV/c
x 1480 -"-
1.0
0.5
b)
Inelastic
1.0
0.5
0.8
1.2
1.6
2.0
2.4
2.8
R (fm)
b_{max} (fm)

Fig. 8

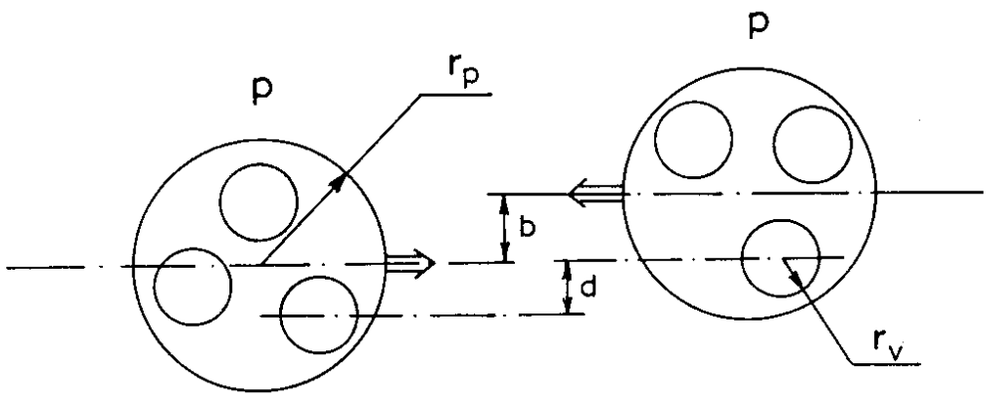

Fig. 9

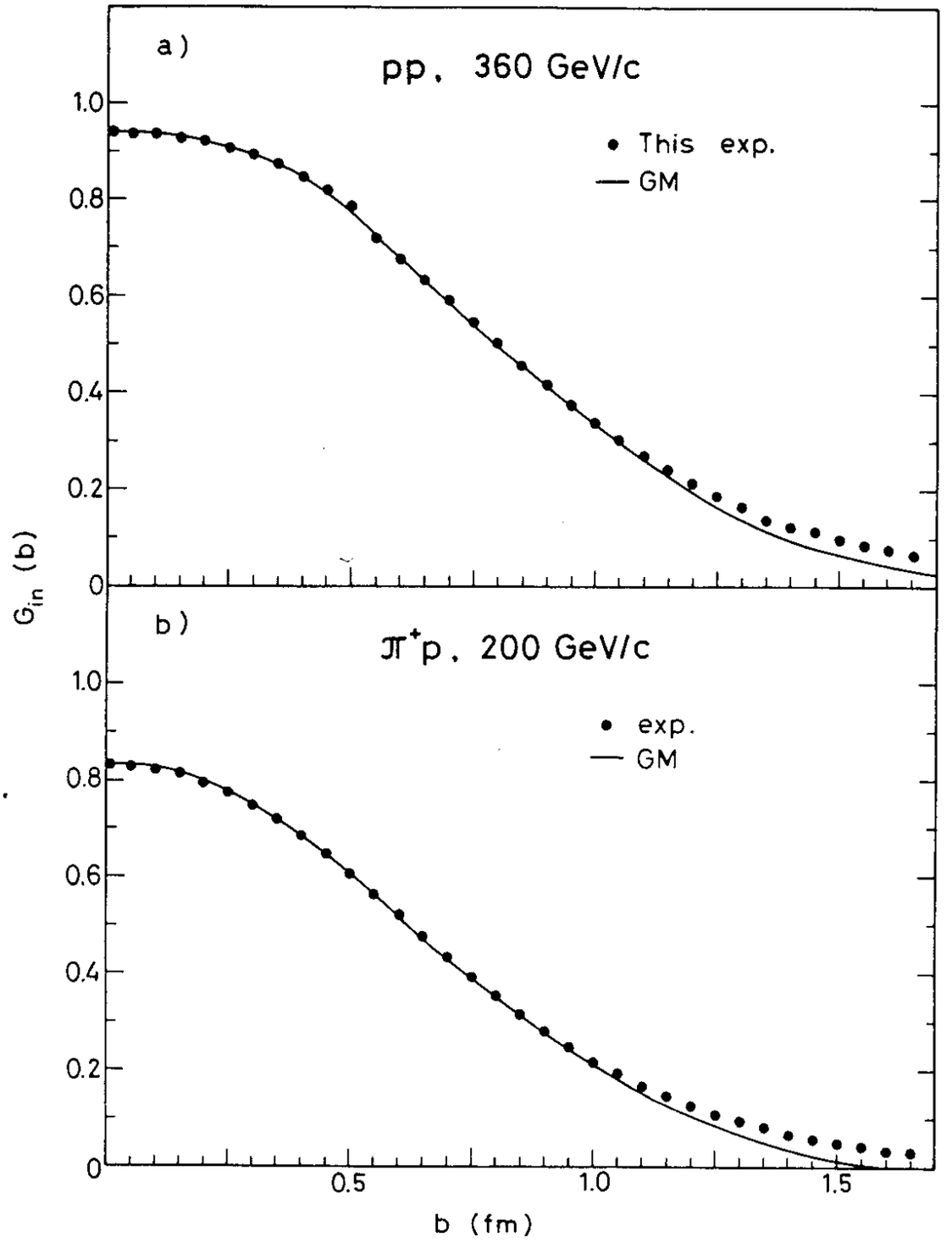
a)
pp, 360 GeV/c
This exp.
GM
b)
π⁺p, 200 GeV/c
exp.
GM
G_in (b)
b (fm)
0
0.2
0.4
0.6
0.8
1.0
0.5
1.0
1.5

Fig. 10

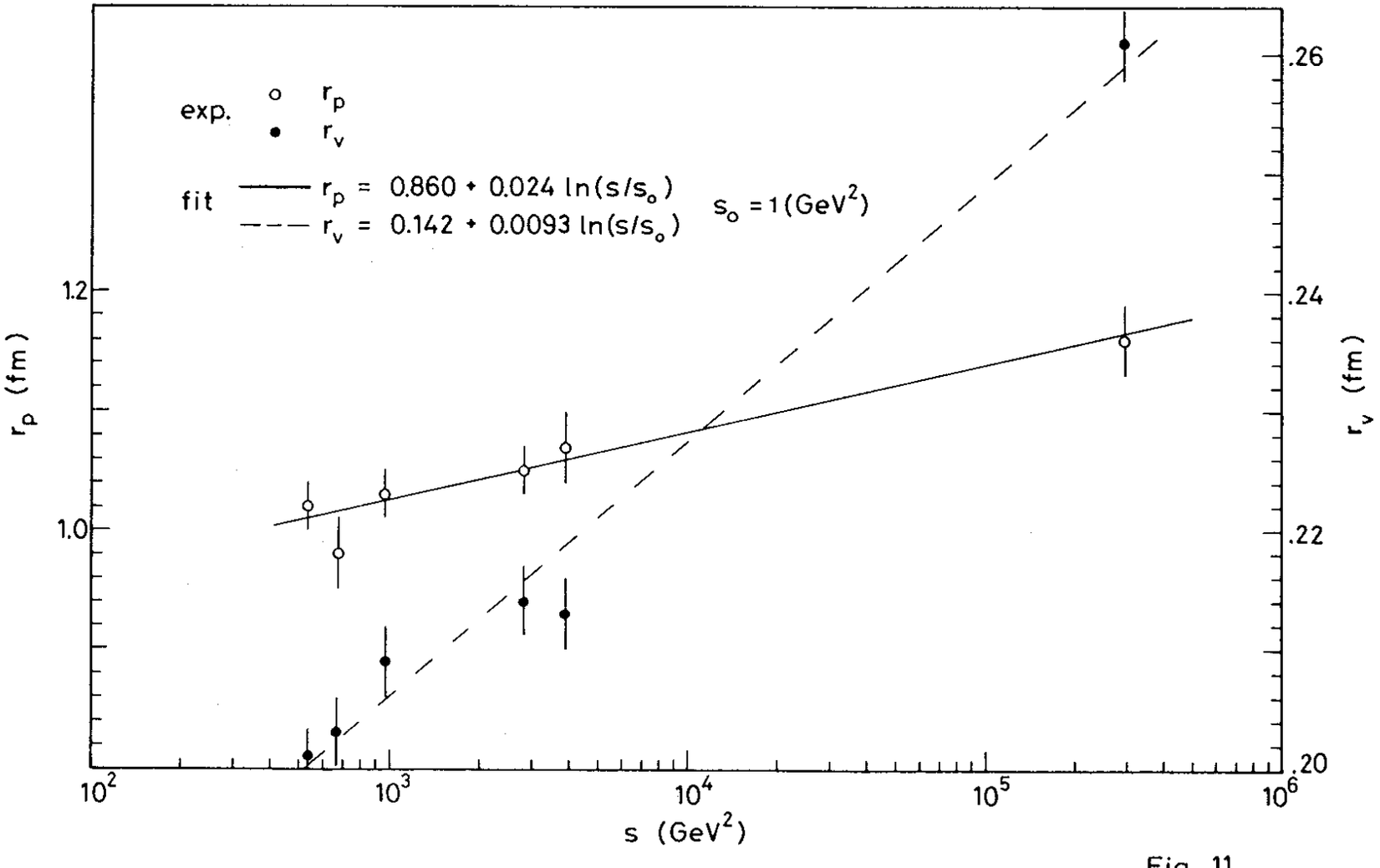
exp.
r_p
r_v
fit
$r_p = 0.860 + 0.024 \ln(s/s_o)$
$r_v = 0.142 + 0.0093 \ln(s/s_o)$
$s_o = 1 (GeV^2)$
1.2
1.0
r_p (fm)
.26
.24
.22
.20
r_v (fm)
10^2
10^3
10^4
10^5
10^6
s (GeV^2)

Fig. 11

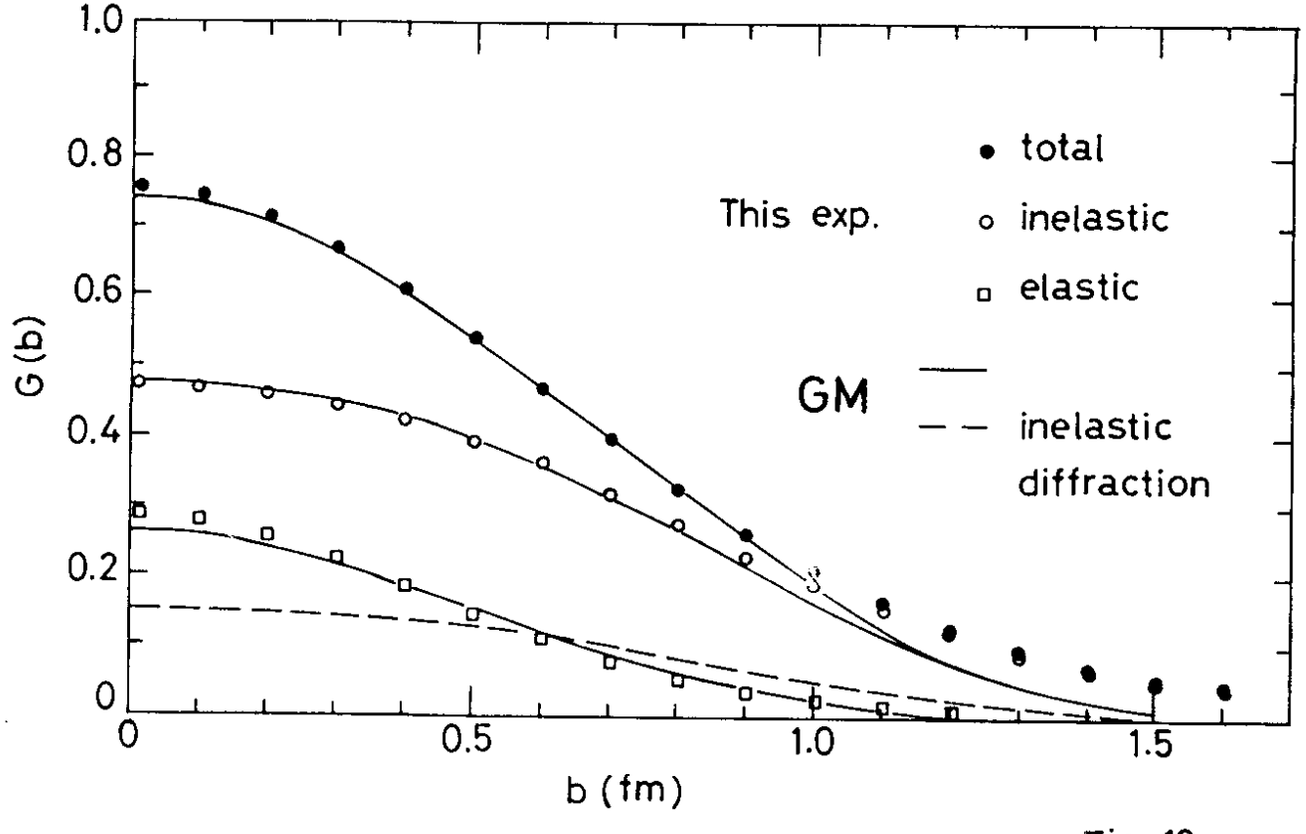
1.0
0.8
0.6
0.4
0.2
0
G(b)
0
0.5
1.0
1.5
b (fm)
This exp.
total
inelastic
elastic
GM
inelastic
diffraction

Fig. 12